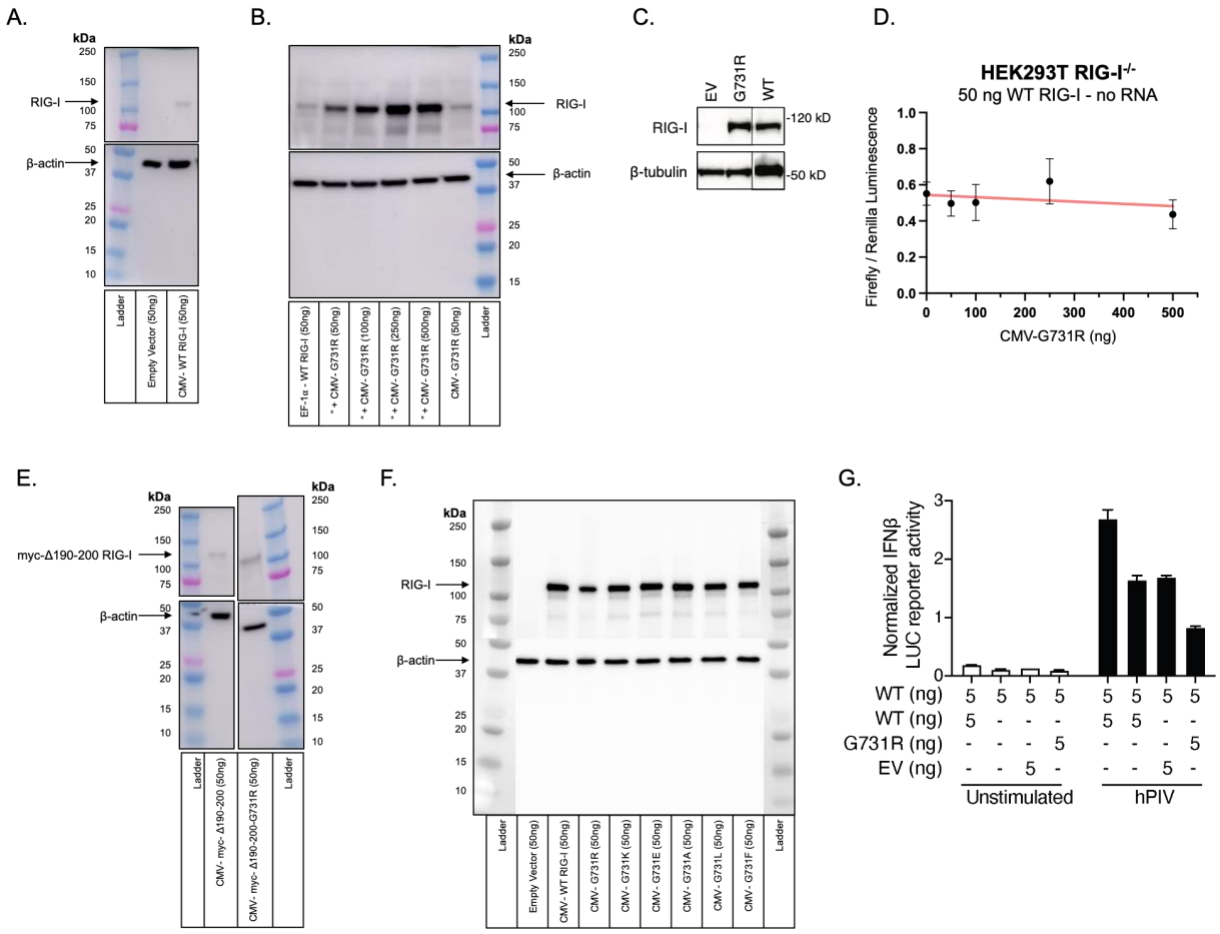

Figure S1. IFN-β reporter assay western blots and control

Western blot corresponding to IFN-β reporter assay in HEK293T RIG-I$^{-/-}$ cells for transient expression of (A) CMV- WT RIG-I, (B) EF1-α- WT RIG-I and competing CMV-G731R, (E) CMV-myc-Δ190-200 constructs, and (F) CMV-G731X mutants relative to β-actin. Panels (A) is related to data in Figure 2G, (B) is related to Figure 3F, (E) is related to Figure 6, and (F) is related to Figure 8.

(C) Immunoblot assessing expression of RIG-I WT and G731R, corresponding to Figure 2H. Cell lysates from transfections with empty vector (EV), RIG-I WT, or RIG-I G731R were resolved on the same gel. A section of the gel between the WT and G731R lanes was removed, as indicated by the black line.

(D) IFN-β response of constitutively expressed WT RIG-I under EF1α promoter measured by dual luciferase reporter assay in the absence of RNA, while titrating G731R plasmid, related to data in Figure 3. Each condition was performed three times (independent RNA transfections, n=3). The plot shown shows the mean values at each protein concentration,

with error bars representing the standard error of the mean (SEM), and the curve shows the hyperbolic decay fit to the mean data.

(G) Cells were co-transfected with WT RIG-I (5 ng) and an equal amount (5 ng) of WT RIG-I, G731R RIG-I, or empty vector (EV) plasmids, and then either left unstimulated or infected with hPIV. IFNβ-driven Firefly luciferase reporter activity for each condition was normalized to *Renilla* luciferase. Data show means ± SD of 2 technical repeats for one representative experiment. Related to Figure 3H.

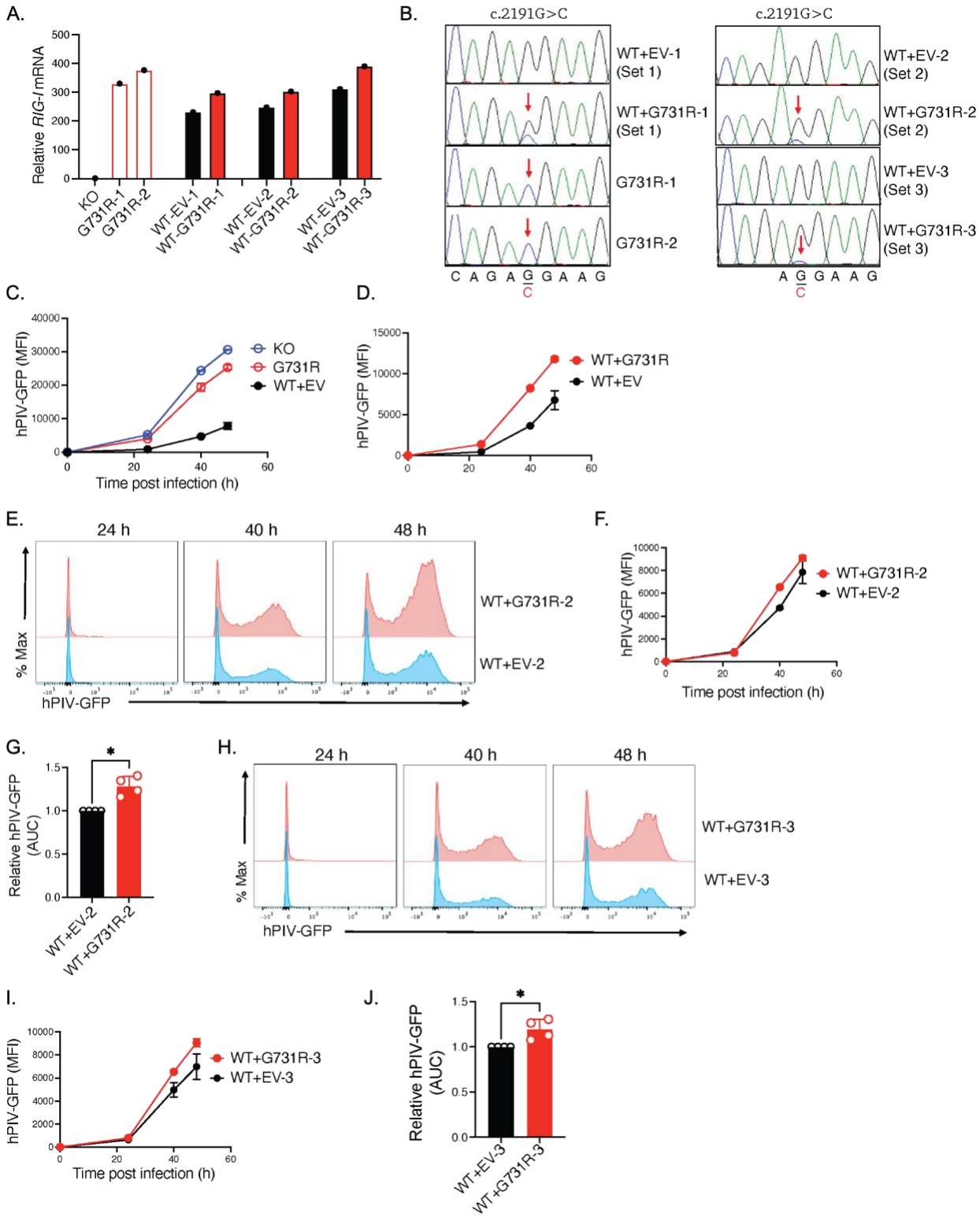
A.
Relative RIG-I mRNA
500
400
300
200
100
0
KO
G731R-1
G731R-2
WT-EV-1
WT-G731R-1
WT-EV-2
WT-G731R-2
WT-EV-3
WT-G731R-3
B.
c.2191G>C
WT+EV-1
(Set 1)
WT+G731R-1
(Set 1)
G731R-1
G731R-2
C A G A G G A A G
C
c.2191G>C
WT+EV-2
(Set 2)
WT+G731R-2
(Set 2)
WT+EV-3
(Set 3)
WT+G731R-3
(Set 3)
A G G A A G
C
C.
hPIV-GFP (MFI)
40000
30000
20000
10000
0
0
20
40
60
Time post infection (h)
KO
G731R
WT+EV
D.
hPIV-GFP (MFI)
15000
10000
5000
0
0
20
40
60
WT+G731R
WT+EV
E.
24 h
40 h
48 h
% Max
hPIV-GFP
WT+G731R-2
WT+EV-2
F.
hPIV-GFP (MFI)
10000
8000
6000
4000
2000
0
0
20
40
60
Time post infection (h)
WT+G731R-2
WT+EV-2
G.
Relative hPIV-GFP
(AUC)
1.5
1.0
0.5
0.0
*
WT+EV-2
WT+G731R-2
H.
24 h
40 h
48 h
% Max
hPIV-GFP
WT+G731R-3
WT+EV-3
I.
hPIV-GFP (MFI)
10000
8000
6000
4000
2000
0
0
20
40
60
Time post infection (h)
WT+G731R-3
WT+EV-3
J.
Relative hPIV-GFP
(AUC)
1.5
1.0
0.5
0.0
*
WT+EV-3
WT+G731R-3

Figure S2. G731R RIG-I interferes with the ability of WT RIG-I to restrict hPIV replication in vitro.

(A) For the KO or transduced cell lines generated as described in Figure 3, expression of *RIGI* mRNA was quantified by qRT-PCR, normalized to *ACTB* and shown relative to that of KO cells. Two sets of independently transduced G731R cells were generated. Three sets of independently transduced WT+G731R or WT+EV cells were generated in parallel.

(B) Sanger dideoxy sequencing chromatograms of cDNA from the generated cell lines at the variant site. Set 1 of WT+G731R and WT+EV was used in Figure 3. In WT+G731R cells, WT *RIGI* was overexpressed compared to mutant *RIGI*.

(C) GFP mean fluorescence intensity (MFI) over time in RIG-I KO fibroblasts alone, or transduced either with RIG-I G731R or WT plus EV (WT+EV) for a representative experiment corresponding to Figure 3C.

(D) GFP mean fluorescence intensity (MFI) over time in human primary RIG-I KO fibroblasts transduced with WT RIG-I plus G731R (WT+G731R) or WT RIG-I plus EV (WT+EV) (Set 1), corresponding to Figure 3E.

(E-G**)** Human primary fibroblasts transduced with WT+G731R or WT RIG-I WT+EV (Set 2) were infected with GFP-tagged hPIV (MOI 0.2) for 24 to 48 h. Representative flow cytometry plots of hPIV-infected cells (E), with corresponding GFP MFI over time (F). hPIV infection was quantified by AUC of GFP MFI and shown relative to that of WT+EV cells in each individual experiment (G).

(H-J) Similar to (E-G), but experiments were performed using WT+G731R or WT+EV cells (Set 3). Data for WT+EV shown in panels (G) and (J) were used for panel (D) in Figure 3E in simultaneously run experiments. Statistical analyses were performed using one-sample t-test (G and J). * $P < 0.05$.

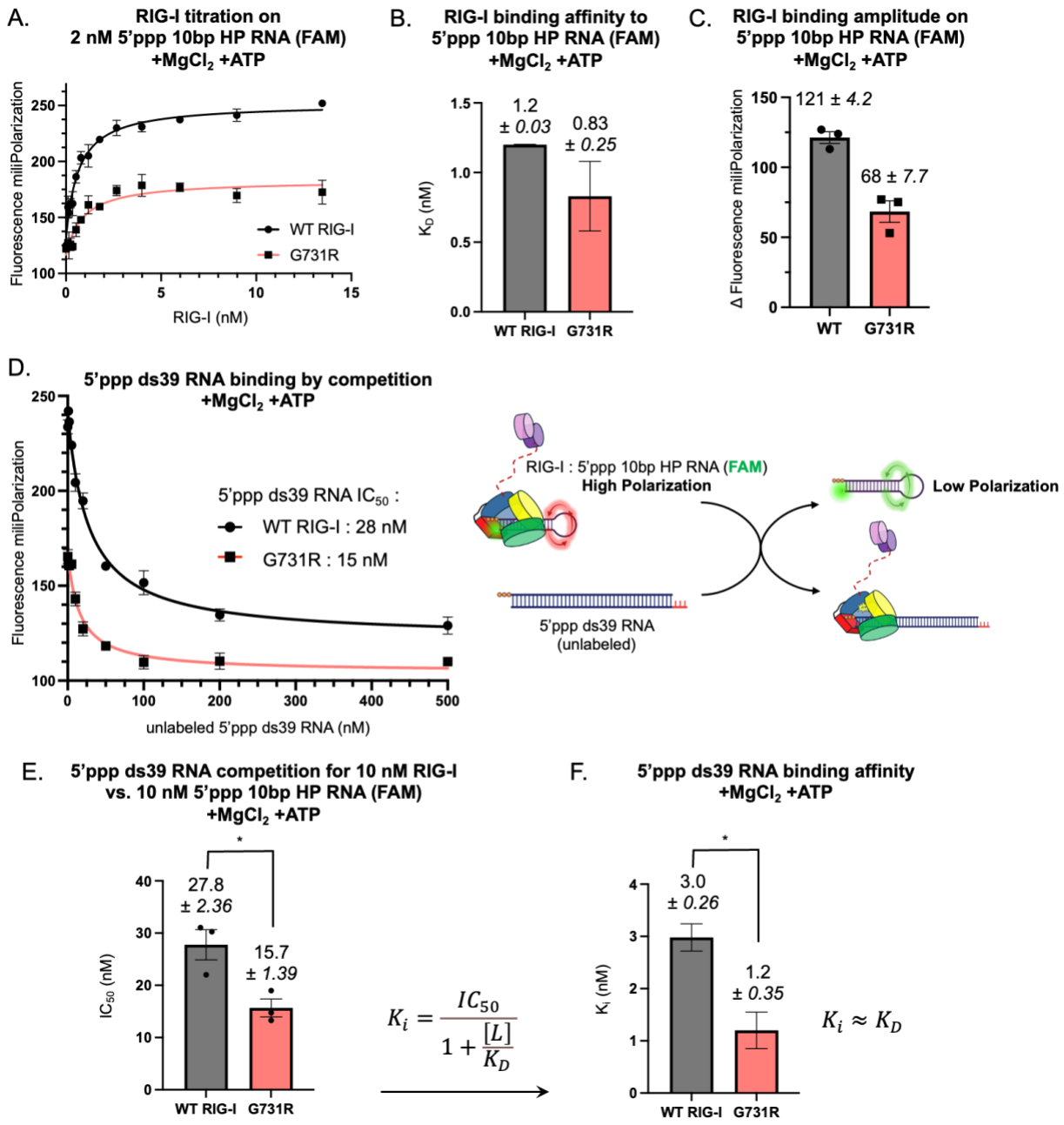

Figure S3. Fluorescence-based RNA binding measurements related to RNA binding data in Figure 3B.

(A) Fluorescence polarization (FmP) of fluorescein-labeled 5'ppp 10bp HP RNA in the presence of increasing protein concentration (biological replicates, n=3). The RNA binding data were fit to equation 2 to obtain the FmP amplitude and the RNA K_D values.

(B) 5’ppp 10bp HP RNA binding affinity (K_D) measured by changes in fluorescence polarization while titrating RIG-I against constant 2 nM RNA. Error bars represent the standard error of the mean (biological replicates, n=3).

(C) The FmP amplitude values from experiments in panel A are compared (biological replicates, n=3).

(D) 5’ppp ds39 RNA binding to WT or G731R was measured by competition assay. Fluorescence polarization of FAM-labeled 5’ppp 10bp HP RNA (10 nM) bound to RIG-I or G731R (10 nM) was measured while titrating in increasing unlabeled 5’ppp ds39 RNA. The data were fit to equation 1 to obtain the half maximal inhibitory concentration IC_{50}. Error bars represent the standard error of the mean (biological replicates, n=3).
(E) 5’ppp ds39 RNA competition (IC_{50}) for RIG-I displacement from 5’ppp 10bp HP RNA as monitored by changes in fluorescence polarization while titrating 5’ppp ds39 RNA against 10 nM equimolar RIG-I-bound 5’ppp 10bp HP RNA (FAM). Error bars represent the standard error of the mean (biological replicates, n=3).

(F) Cheng-Prusoff equation is used to obtain 5’ppp ds39 RNA K_i values, which are representative of RIG-I’s binding affinity for 5’ppp ds39 RNA (K_D). Error bars represent the propagated standard error of the means. Statistical analysis was performed using unpaired t-test. *, $P<0.05$.

Consolidated HDX differential peptide coverage

			Δ HDX				
Domain	**Feature**	**Peptide Sequence**	Start Residue	End Residue	wt RIG-I ± 5'ppp 10bp HP RNA	apo G731R vs. WT RIG-I	G731R ± 5'ppp 10bp HP RNA
CARD1 (1-91)		FQDYIRKTLDPTYIL	11	25	15 (4)	2 (3)*	-17 (2)
		FQDYIRKTLDPTYILS	11	26	15 (4)	-1 (2)*	-21 (3)
		YIRKTLDPTYIL	14	25	15 (5)	2 (2)*	-20 (3)
		SYMAPWFREEEVQ	26	38	17 (4)	1 (2)*	-30 (3)
		YIQAEKNNKGPMEAATL	39	55	11 (4)	-6 (3)	-28 (3)
		LKFLLE	57	62		0 (1)*	2 (2)*
		QEEGWFRGFLDA	64	75	13 (5)	-8 (2)	-17 (3)
		DALDHAGYSGL	74	84	8 (2)	-6 (3)	-22 (4)
		DALDHAGYSGL	74	84	12 (2)	-6 (2)	-21 (4)
		YEAIESWD	85	92	16 (5)	2 (2)*	-28 (4)
CARD2 (92-185)		FKKIEKLEE	93	101	-4 (7)*	-5 (3)	-40 (3)
	CARD2:Hel2i latch (100-115)	YRLLL	102	106	11 (3)	6 (3)	
		KRLQPEF	107	113	6 (4)	6 (2)	-27 (3)
		KTRIPTDMSDL	114	126	17 (4)	1 (3)*	-33 (3)
		KTRIPTDMSDL	114	126	17 (3)	-2 (3)*	-38 (2)
	CARD2:Hel2i latch (145-150)	LNQECEE	130	137		-2 (2)*	-21 (5)
		ILQICSTKGMMAGAEKLVE	138	156	22 (3)	2 (2)*	-19 (4)
		ILQICSTKGMMAGAEKLVE	138	156	16 (4)	2 (1)*	-14 (3)
		LRSDKENWPKTLKLAL	159	174	22 (8)	3 (2)*	-30 (2)
		LRSDKENWPKTLKLAL	159	174		3 (2)*	-29 (4)
		ALEKERNKFSEL	173	184	8 (4)	1 (3)*	-37 (5)
ID Linker (185-244)	Electrostatic gate (190-220)	WIVEKGIKDVETEDL	185	199	2 (4)*	-8 (2)	-57 (5)
		WIVEKGIKDVETEDLEDKMETSD	185	207	1 (2)*		-46 (6)
		EDKMETSDIQIF	200	211	4 (6)*		-25 (3)
		YQEDPECQNL	212	221	3 (4)*	-0 (3)	-54 (7)
		SENSCPPSEVSDTNL	222	236	4 (4)*	-7 (2)	-80 (4)
		VSDTNL	231	236	2 (3)*	-15 (3)	-88 (5)
		YSPFKPRN	237	244	0 (9)*	-12 (2)	-66 (4)
		YSPFKPRNYQLE	237	248	0 (6)*		-55 (4)
		LALPAMKGKNTICAPTGCGKTFVSL	249	274	-1 (3)*	-3 (2)*	-23 (2)
		TICAPTGCGKTF	259	270	2 (5)*	-5 (1)*	-56 (4)
	RNA binding motifs	LICEHHLKKFPQGQKGKVVF	275	294		-1 (1)*	-23 (2)
Hel1 (244-455)		FANQIPVYE	295	303	-16 (4)	-11 (3)	
	motif Ia (300-330)	FERHGYRVTGISGATAENVPVEQ	313	335	-3 (6)*	-4 (2)*	-54 (4)
		FERHGYRVTGISGATAENVPVEQ	313	335	-2 (7)*	-5 (1)*	-37 (2)
		IVENND	336	341	-2 (2)*	1 (2)*	-7 (3)
	motif Ic (340-370)	IILTPQIL	342	350	-9 (4)	3 (2)*	-7 (3)
		IILTPQILVNNLKKGTIPSL	342	362	-12 (5)	-1 (2)*	-26 (3)
		LVNNLKKGTIPSLSIF	351	365	-7 (4)	-2 (2)*	-26 (3)
	motif IIa (370-390)	MIFDECHNTSKQHPYNM	366	384	-9 (4)	-1 (2)*	-22 (2)
		IFDECHNTSKQHPYNMIM	369	386	-7 (3)	2 (1)*	-20 (2)
		DECHNTSKQHPYNMIM	371	386	-9 (4)	0 (1)*	-27 (3)
		FNYLDQKLGGSSGPLPQVRGL	387	407	0 (2)*	2 (1)*	-22 (2)
		FNYLDQKLGGSSGPLPQVRGL	387	407	0 (2)*	2 (1)*	-20 (2)
		TASVGVGDAIKNTDEAL	408	423	-4 (3)*	-2 (2)*	
		DYICKL	424	429		3 (2)*	2 (5)*
		DASVIATVKHNLEEL	434	448	0 (3)*	0 (3)*	-8 (2)
		SVIATVKHNLEEL	436	448	-1 (4)*	1 (3)*	-12 (2)
Hel2 (245-469)...	Insertion domain linker	LEQVVYKPQKF	448	458	-4 (5)*	-2 (3)*	-41 (5)
		LEQVVYKPQKF	448	458	-3 (5)*	1 (3)*	-36 (4)
		EQVVYKPQKF	449	458	-4 (5)*	0 (3)*	-28 (3)
Hel2i (470-607)		FRKVESRISDKFKYIAQL	459	477		-1 (2)*	-20 (2)
		MRDTESLAKRICKDLENL	478	495		-2 (2)*	-13 (3)
		AKRICKDLENL	485	495	-7 (5)	-2 (3)*	-21 (5)
	RNA binding region (505-520)	SQIQNREFGTQKYEQW	496	511	-4 (4)*	0 (2)*	-43 (4)
		IVTVQKACM	512	520	-2 (2)*	-7 (2)	-3 (4)*
		IVTVQKACM	512	520	-1 (5)*		-1 (2)*
	CARD2/CTD :Hel2i latch (520-540)	VFQMPDKDEESRICKA	521	536	-12 (5)	-4 (3)*	-21 (3)
		VFQMPDKDEESRICKA	521	536	-10 (4)	-1 (3)*	-29 (3)
		VFQMPDKDEESRICKALF	521	538	-9 (4)	-2 (2)*	-22 (3)
		LYTSHLRKYNDAL	539	551	0 (1)*	2 (1)*	2 (2)*
	CARD2:Hel2i latch (565-580)	DALIISEHARMKD	549	561	1 (3)*	0 (1)*	-8 (2)
		HARMKDALD	556	564	8 (58)	-1 (1)*	-12 (3)
		HARMKDALD	556	564	8 (49)	-1 (1)*	-14 (4)
		YLKDFFSNVRAAGF	565	578	10 (3)	-1 (2)*	-25 (3)
		ESVSRDPSNENPKLED	597	612	1 (4)*	-3 (2)*	-28 (3)

Consolidated HDX differential peptide coverage (cont.)

Δ HDX							
Domain	**Feature**	**Peptide Sequence**	Start Residue	End Residue	wt RIG-I ± 5'ppp 10bp HP RNA	apo G731R vs. WT RIG-I	G731R ± 5'ppp 10bp HP RNA
Hel2 (608-743)	RNA binding motifs	VSRDPSNENPKLEDLCF	599	615	-2 (3)*	-1 (3)*	-24 (2)
		FILQEEYHLNPET	615	627	0 (4)*	-2 (2)*	-10 (2)
		ILQEEYHLNPET	616	627	-1 (2)*	-1 (2)*	-13 (2)
	motif IV (630-695)	VKTRALVDALKN	633	644	-7 (2)	-3 (1)*	-15 (3)
		ALKNWEGNPKL	641	652	1 (3)*	-2 (2)*	-13 (2)
		ALKNWEGNPKL	641	652	1 (3)*	-1 (2)*	-12 (2)
		SFLKPGIL	653	660	-8 (2)	1 (2)*	-18 (3)
		TGRGKTNQNTGWTLPAQKCIL	661	681	-9 (4)	-11 (2)	-61 (3)
		DAFKASGDHNIL	682	693	-9 (3)	0 (3)*	-53 (4)
		DAFKASGDHNIL	682	693	-9 (3)	-5 (2)*	-42 (3)
		FKASGDHNIL	684	693	-8 (3)	0 (2)*	-35 (3)
		FKASGDHNIL	684	693	-8 (3)	0 (2)*	-34 (2)
	motif V (695-720)	IATSVADEGID	694	704	-14 (3)	-5 (2)*	-41 (5)
		IATSVADEGID	694	704	-13 (4)	-4 (2)*	-35 (3)
		IAQCNL	705	710	-7 (4)	-3 (3)*	-40 (3)
		VILYE	711	715	-1 (1)*	1 (2)*	-2 (3)*
		YEYVGNVIKM	714	723	-14 (4)	-4 (3)*	-38 (3)
		FLLTSNA	738	744	-9 (5)	-6 (1)	-33 (3)
Pincer (744-803)	Helicase bridge / CTD linker	LTSNAGVIEKEQINM	740	754	-3 (4)*	-8 (3)	-19 (4)
		YKEKMMNDSIL	755	765	0 (1)*	5 (2)*	-7 (2)
		QTWDEAVF	768	775	-1 (3)*	-1 (2)*	-41 (4)
		WDEAVF	770	775	1 (2)*	-1 (3)*	-18 (2)
CTD (804-925)		VRVEECHY	822	830	-2 (4)*	-2 (1)*	-14 (2)
		TVLGDA	831	836	0 (3)*		-20 (3)
	5' capping loop (840-860)	TVLGDAFKECF	831	841	-2 (4)*	0 (2)*	
		VSRPHPKPKQFSSF	842	855		-6 (1)	-38 (3)
		CARQNCSHDWGIHVKYKTFEPVIKESF	863	891		-1 (1)*	-9 (3)
	RNA binding region (880-905)	VVEDIATGVQTL	892	903	-11 (3)	-6 (3)	-30 (3)
		DIATGVQTL	895	903	-10 (3)	-8 (3)	-28 (6)
		YSKWKDFHF	904	912		-6 (2)	-33 (3)
		EKIPFDPAEMSK	913	924	-2 (3)*	-7 (2)	-38 (5)
		EKIPFDPAEMSK	913	924	-1 (4)*	-7 (2)	-53 (3)

Figure S4. Annotated mapping of consolidated HDX differential peptide coverage related to data in figure 4.

Chart summarizing the differential HDX patterns of specific peptides of RIG-I from each experimental condition, annotated by protein domain and functional features.

Figures S5-S10. Hydrogen-Deuterium Exchange Mass Spectroscopy sequence coverage heatmaps related to the data in Figure 4.

Time-consolidated HDX data is shown using a perturbation view from HDX Workbench (Scripps Research Institute, 2024). Individual peptides are represented by horizontal strips below their respective portions of the protein sequence, with values indicating percent deuterium uptake ± standard deviation. Individual peptides are colored according to the colorimetric perturbation key shown.

Figure S5. HDX sequence coverage for WT RIG-I apo (from G731R vs WT RIG-I experiment)

Figure S6. HDX sequence coverage for G731R apo (from G731R vs WT RIG-I experiment)

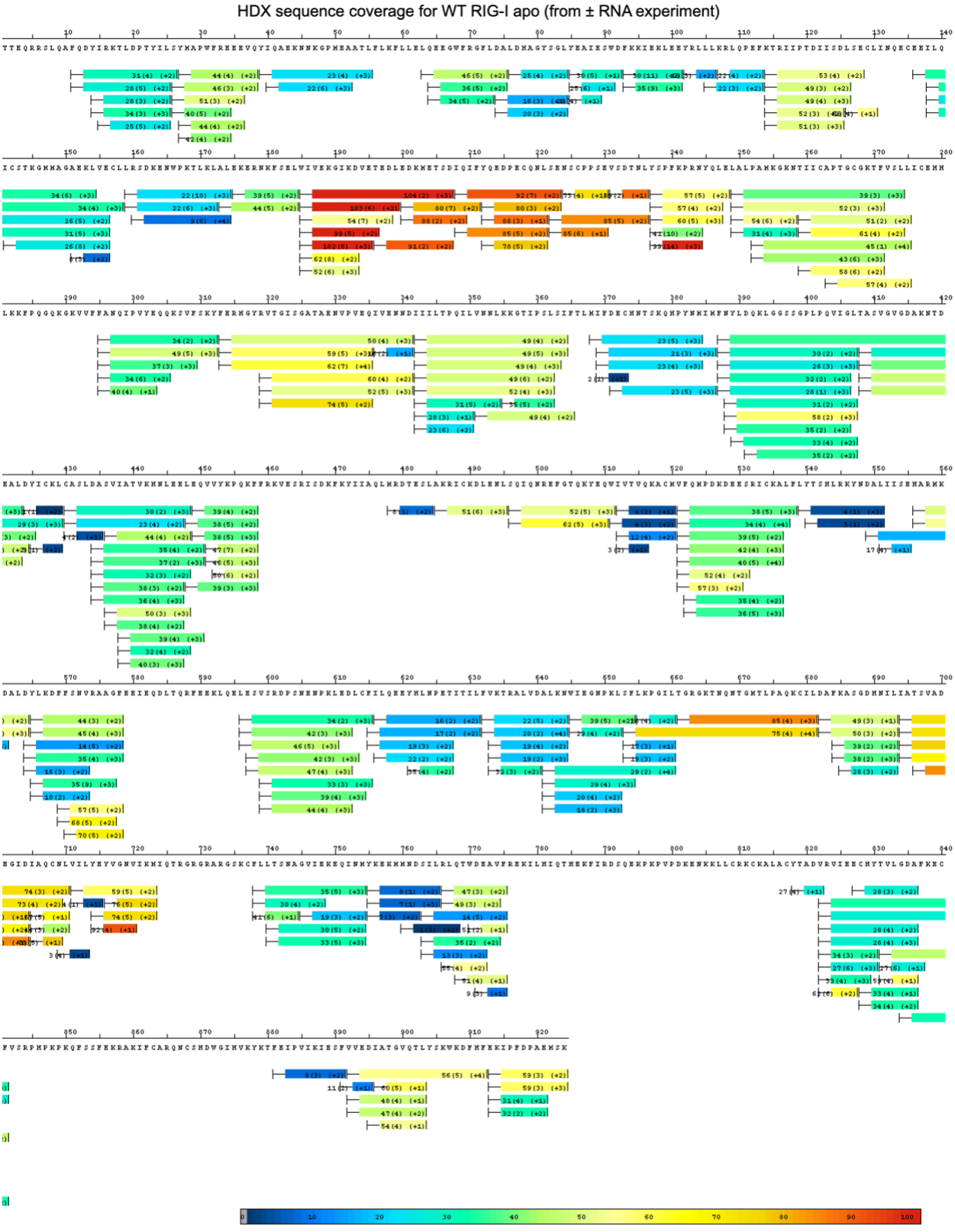

Figure S7. HDX sequence coverage for WT RIG-I apo (from ± RNA experiment)

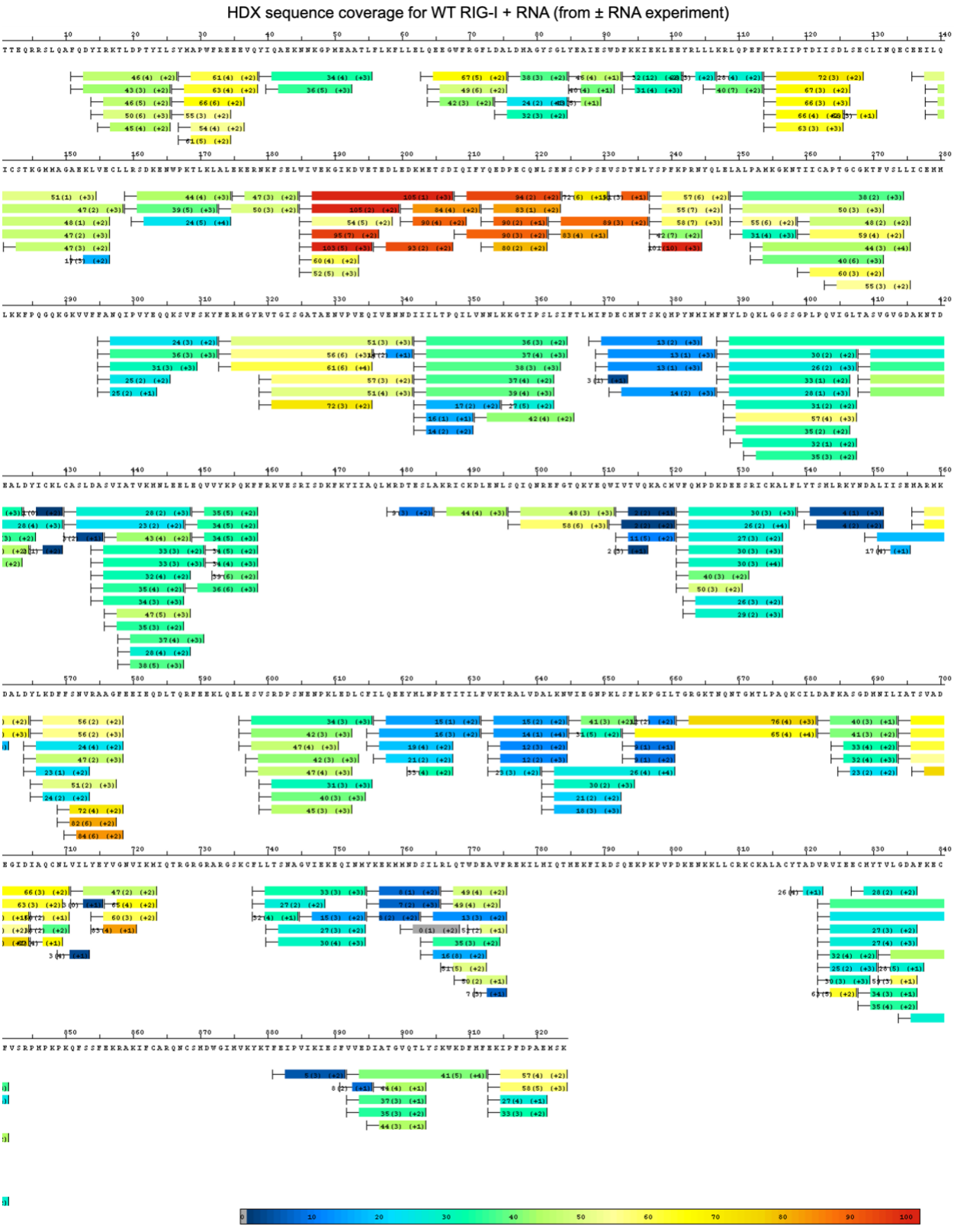

Figure S8. HDX sequence coverage for WT RIG-I + RNA (from ± RNA experiment)

Figure S9. HDX sequence coverage for G731R apo (from ± RNA experiment)

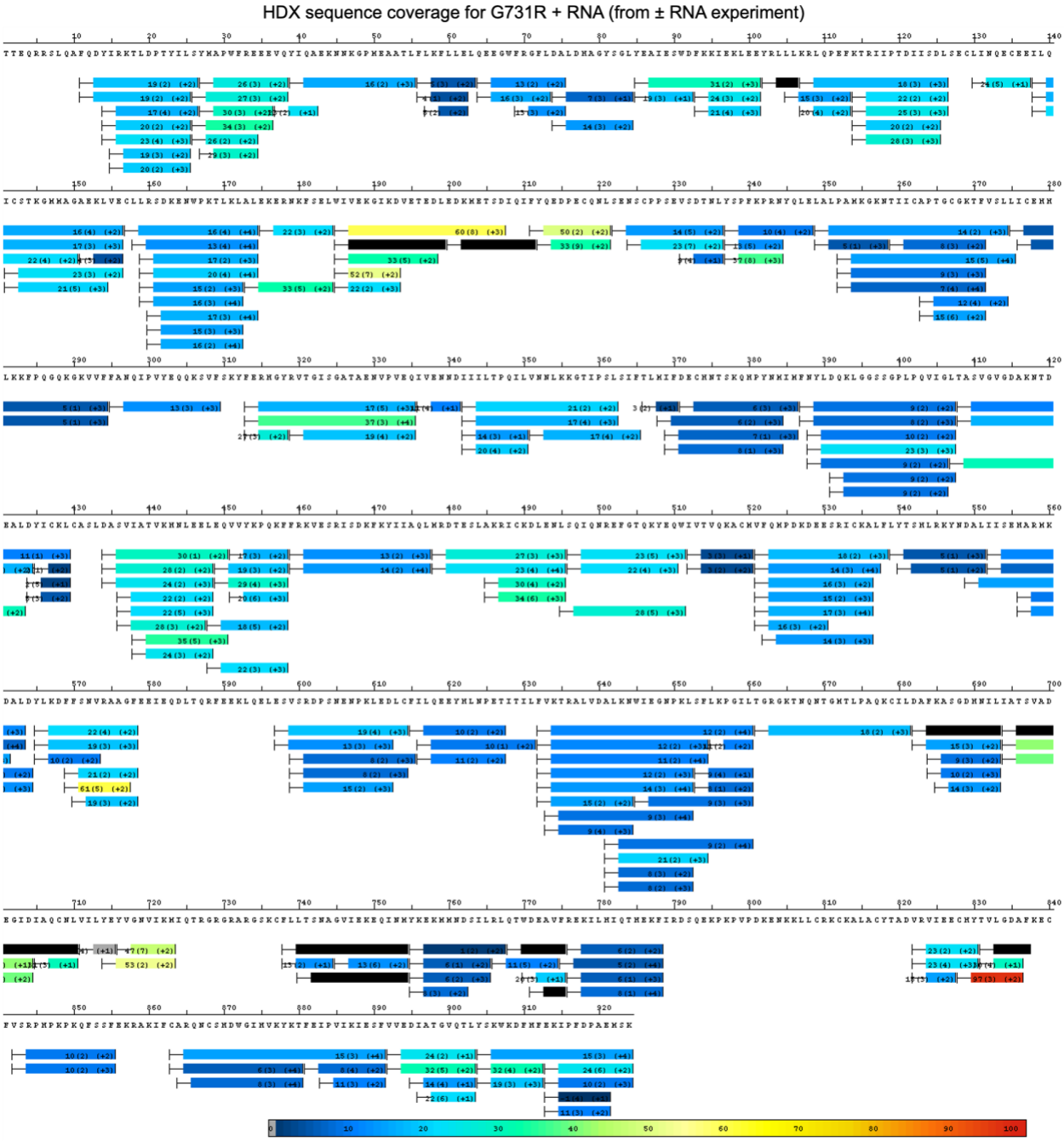

Figure S10. HDX sequence coverage for G731R + RNA (from ± RNA experiment)

Data is representative of two biological replicates.

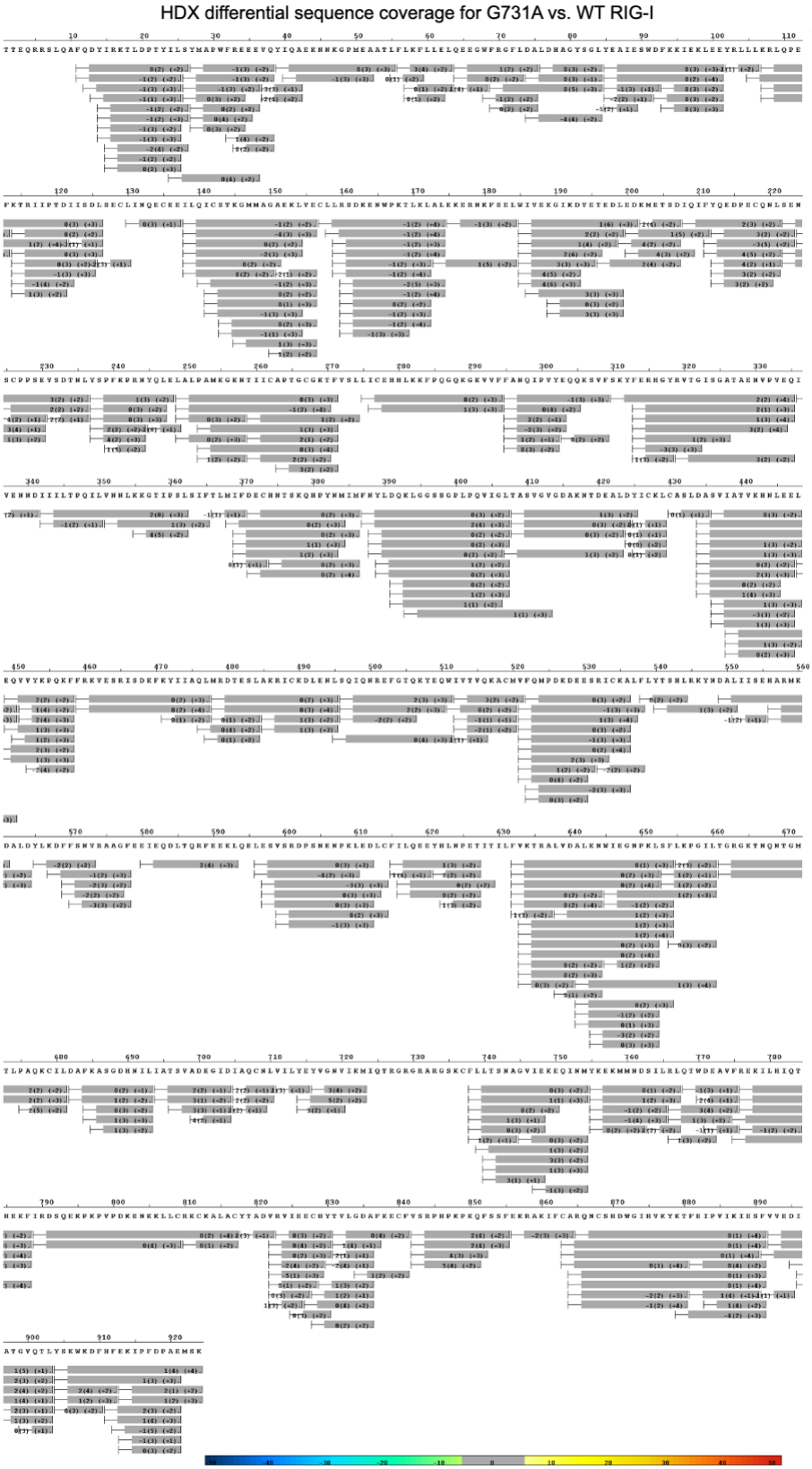

Figure S11. HDX differential sequence coverage for G731A vs. WT RIG-I

Figure S12. HDX differential sequence coverage for G731A ± RNA

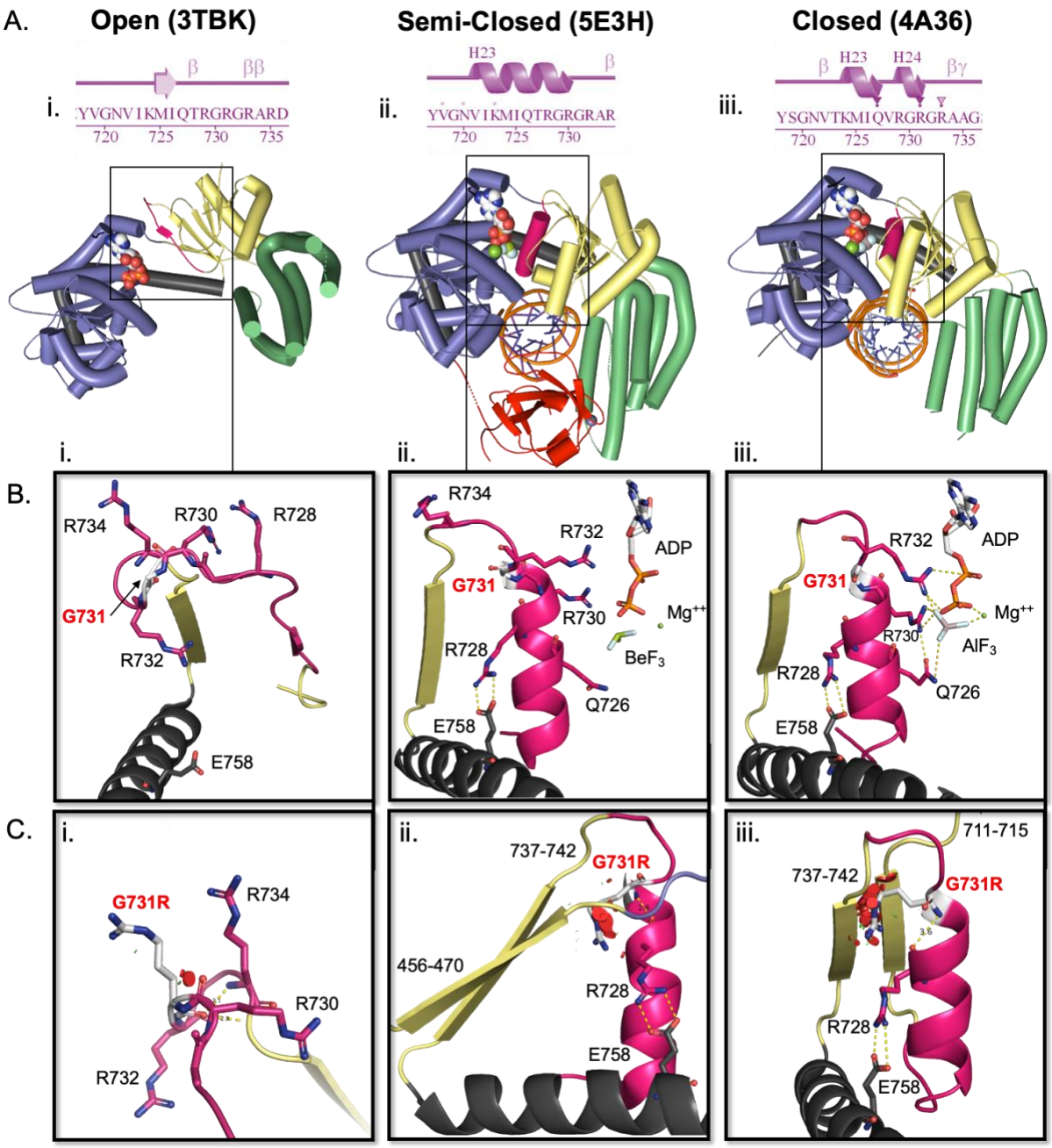

Figure S13. Conformational changes in RIG-I from open to closed states upon RNA binding

(A) PDBsum linear representation of secondary structure formation in motif VI (in pink) of (i) open mouse RIG-I helicases (PDB: 3TBK), (ii) semi-closed human RIG-I (PDB: 5E3H), and (iii) closed duck RIG-I helicases (PDB: 4A36). Below are front top views of RIG-I crystal structures captured in each conformational state. Structures are aligned by the Hel1 domain.

(B) Zoomed in view of each respective RIG-I structure showing the isolated motif VI and associated interactions in detail.

(C) PyMOL Mutagenesis Wizard analysis of G731R computational mutation in each respective structure. The red disks indicate pairwise overlap of atomic van der Waals radii.

Table S1: Whole Genome Sequencing analysis summary (see excel file)

Table S2: RNA binding constants from fluorescence polarization experiments in Figures 3B and S2.

RNA	constant	WT RIG-I	G731R
5'ppp 10bp HP (FAM)	K_D	1.2 ± 0.03 nM	0.83 ± 0.25 nM
5'ppp ds39	IC_{50}	27.8 ± 2.4 nM	15.7 ± 1.4 nM
5'ppp ds39	K_i	3.0 ± 0.3 nM	1.2 ± 0.4 nM

Table S3: Kinetic parameters from RNA off-rate experiments in Figures 5 C-E.

	WT		G731R		
	CTD	Helicase	CTD	Helicase	
k_{off} (s^{-1})	0.141 ± 0.011	0.0045 ± 0.00006	0.147 ±0.015	0.0062 ± 0.003	- ATP
Kinetic mode population (%)	75.1 ± 4.26	24.9 ± 4.26	92.4 ± 2.03	7.6 ± 2.03	
Kinetic mode lifetime (s)	7.1 ± 0.5	223 ± 2.8	6.7 ± 0.7	198 ± 76.0	
R^2	0.9829 ± 0.01123		0.9814 ± 0.01063		
k_{off} (s^{-1})	0.128 ± 0.012	0.0105 ± 0.001	0.137 ± 0.010	0.0096 ± 0.006	+ ATP
Kinetic mode population (%)	76.7 ± 0.99	23.3 ± 0.99	95.2 ± 0.74	4.8 ± 0.74	
Kinetic mode lifetime (s)	7.9 ± 0.7	96 ± 10.9	7.4 ± 0.5	176 ± 127	
R^2	0.9875 ± 0.007793		0.9822 ± 0.007674		

Table S4: Computational predictions and experimentally determined biochemical impacts of selected G731 missense mutations.

Genomic DNA change	cDNA change	Protein variant	Original	Nucleotide changed	CADD score	AlphaMissense score	AlphaMissense class	MAF in gnomAD	IFNβ reporter activity (relative to WT)
Chr9:32466433C>G	c.2192G>C	p.Gly731Ala	GGA	GCA	24.2	0.308	likely_benign	0	GOF
Chr9:32466433C>T	c.2192G>A	p.Gly731Glu	GGA	GAA	25.7	0.97	likely_pathogenic	6.24E-07	LOF
Chr9:32466434C>G	c.2191G>C	p.Gly731Arg	GGA	CGA	25.5	0.973	likely_pathogenic	Novel (this report)	LOF
Chr9:32466434C>T	c.2191G>A	p.Gly731Arg	GGA	AGA	25.7	0.973	likely_pathogenic	0	LOF
Chr9:32466433C>A	c.2192G>T	p.Gly731Val	GGA	GTA	25.3	0.836	likely_pathogenic	0	Not tested
	-	p.Gly731Leu	GGA	CTA	-	0.926	likely_pathogenic	-	GOF
	-	p.Gly731Phe	GGA	TTT	-	0.983	likely_pathogenic	-	Partial LOF
	-	p.Gly731Lys	GGA	AAA	-	0.991	likely_pathogenic	-	LOF

Table S1: Whole Genome Sequencing analysis summary

Table S2: RNA binding measurements of WT RIG-I and G731R by fluorescence polarization were determined from experiments shown in figures 3B and S2.

Table S3: RNA unbinding measurements of WT RIG-I and G731R by stopped-flow fluorescence intensity were determined from experiments shown in figure 5 C,D,E.

Table S4: Computational predictions and experimentally determined biochemical impacts of selected G731 missense mutations.

MAF: Minor Allele Frequency, CADD: Combined Annotation Dependent Depletion, LOF: Loss of Function, GOF: Gain of Function

Table S5: Oligonucleotides

5’ppp ss39 non-template ssDNA 5’- CAG TAA TACGAC TCA CTA TTA GTT GGT GGT TGT TGT GTG TTT GTG GTT GGT TTG TTT GG -3’	IDT
5’ppp ss39 template ssDNA 5’- GTC ATT ATG CTG AGT GAT AAT CAA CCA CCA ACA CAC AAA CAC CAA CCA AAC AAA CC -3’	IDT
5’ppp ss39 RNA 5’- AGU UGG UGG UUG UUG UGU GUU UGU GGU UGG UUU GUU UGG -3’	In vitro transcription
5’ppp 24Pal non-template ssDNA 5’- TAA TAC GAC TCA CTA TA GGA ACT TAT CTA TAG ATA AGT TCC -3’	IDT
5’ppp 24Pal template ssDNA 5’- mGmGA ACT TAT CTA TAG ATA AGT TCC TA TAG TGA GTC GTA TTA -3’	IDT
5’ppp 24Pal RNA 5’ – GGA ACU UAU CUA UAG AUA AGU UCC – 3’	In vitro transcription
ss39 RNA complement (FAM) 5’- dT[Fam-dT]dT CCA AAC AAA CCA ACC ACA AAC ACA CAA CAA CCA CCA ACU -3’	Dharmacon
ss39 RNA complement 5’- dTdTdT CCA AAC AAA CCA ACC ACA AAC ACA CAA CAA CCA CCA ACU -3’	Dharmacon
5’ppp 10bp HP RNA (FAM) 5’-pppGAAUAUAAUAGUGAUAUUAUAUUC[FAM]-3’	TriLink
5’ppp s27 RNA 5’-pppAUAGCUCCUGAUAGUUAGUAUCCAUCG-3’	Biosynthesis
Complementary ss27 RNA (DY547) 5’-Bi-CGAUGGAUACUAACUAUCAGGACGUAU[DY547]-3’	Dharmacon
ss26 RNA chi (for ds26 Stem RNA): 5’ dA dT dA dC dG UCC UGA UAG UUA GUA UC dC dA dT dC 3’	Dharmacon
ss26 RNA chi (3’ FAM) (for ds26 Stem RNA): 5’ dC dG dA dT dG GAU ACU AAC UAU CAG GA dC dG (dT-FAM) dA 3’	Horizon Discovery
RIG-I crRNA-1, 5’-AATTCCCACAAGGACAAAAG-3’	IDT
RIG-I crRNA-2, 5’-AGGTTGTTCACAAGAATCTG-3	IDT
RIG-I crRNA-3, 5’-GGCATCCCCAACACCAACCG-3’	IDT
IFNB1 RT forward primer 5’- AGGATTCTGCATTACCTGAAGG -3’,	IDT
IFNB1 RT reverse primer 5’- GGCTAGGAGATCTTCAGTTTCG -3’	IDT
ACTB RT forward primer 5’-ACCTTCTACAATGAGCTGCG-3’	IDT
RIG-I RT forward primer 5’- TGGCATATTGACTGGACGTG-3’	IDT
RIG-I RT reverse primer 5’-CACTGGCTTTGAATGCATCC-3	IDT

RIG-I G731R cDNA sequencing forward primer 5'-GATTGCCACCTCAGTTGCTG-3'	IDT
RIG-I G731R cDNA sequencing reverse primer 5'-TCCCATGTCTGAAGGCGTAA-3'	IDT
RIG-I G731R gDNA sequencing forward primer 5′-ACCAGCATTACTAGTCAGAAGGA -3′	IDT
RIG-I G731R gDNA sequencing reverse primer 5′-ACAGCTCAACTTTCCTGGGA -3′	IDT